

A toy model of galaxy formation: the importance of mergers, the role of feedback and environmental effects

A. Cattaneo^{1*,2,3}, G. A. Mamon^{2,4}, K. Warnick³, A. Knebe^{3,5}

¹Centre de Recherche Astrophysique de Lyon, 9 av. Charles André, 69561 Saint Genis Laval cedex, France

²Institut d'Astrophysique de Paris (UMR 7095: CNRS & UPMC), 98 bis Boulevard Arago, 75014 Paris, France

³Astrophysikalisches Institut Potsdam, an der Sternwarte 16, 14482 Potsdam, Germany

⁴Astrophysics & BIPAC, Department of Physics, University of Oxford, Keble Rd, Oxford OX1 3RH, UK

⁵Departamento de Física Teórica, Modulo C-XI, Universidad Autonoma de Madrid, 28049 Cantoblanco, Madrid, Spain

*cattaneo@obs.univ-lyon1.fr

31 May 2019

ABSTRACT

We present a toy model of the growth of galaxies within dark matter haloes via gas accretion and mergers. We begin with sub-halo merger trees from a very high-resolution dark matter cosmological simulation. Three physical processes cause the evolution of the baryons to differ from that of the dark matter by suppressing gas accretion and star formation: gravitational shock heating coupled to black hole feedback above a critical halo mass of $M_{\text{shock}} \sim 10^{12} M_{\odot}$; the reionisation of the intergalactic medium in haloes with circular velocities below $v_{\text{reion}} \sim 40 \text{ km s}^{-1}$; stellar feedback in haloes below $v_{\text{SN}} \sim 120 \text{ km s}^{-1}$.

Designed to reproduce the present-day stellar mass function of galaxies, our model matches reasonably well the evolution of the cosmic stellar density. It also predicts a gap between the masses of central and satellite galaxies in agreement with recent SDSS observations: in low-mass haloes the mass function is highly peaked in the narrow range of central galaxy masses, whereas high-mass haloes (massive groups and clusters) contain a much more numerous satellite population.

Gas accretion is the dominant growth mechanism at $m_{\text{stars}} \lesssim m_{\text{crit}} \sim \Omega_{\text{b}}/\Omega_{\text{m}} M_{\text{shock}} \sim 10^{11} M_{\odot}$, while galaxies with $m_{\text{stars}} > m_{\text{crit}}$ acquire most of their final mass through mergers (mostly major and dry). ‘Cold mode’ mergers (mergers in haloes with $M_{\text{halo}} < M_{\text{shock}}$) are rare. Their contribution to galaxy growth is small at all masses but has a maximum at $\sim 10^{10.5} h^{-1} M_{\odot}$. We thus predict a characteristic mass scale of the same order for ULIRGs and quasar hosts.

The different accretion histories of galaxies below and above $m_{\text{stars}} \sim m_{\text{crit}}$ explain why galaxies in the cold mode (i.e. blue star-forming galaxies) are usually spirals and galaxies in the hot mode (i.e. red passive galaxies) are usually ellipticals (assuming that gas accretion forms discs and mergers form spheroids). However, the contribution of mergers to the final stellar masses of galaxies with $m_{\text{stars}} < 10^{11} M_{\odot}$ is low even in satellite galaxies of groups and clusters. Thus, red galaxies with $m_{\text{stars}} < m_{\text{crit}}$, which include dwarf spheroidals and galaxies commonly referred to as dwarf ellipticals, should have structural and kinematical properties that separate them from giant ellipticals.

Key words: galaxies: clusters — galaxies: ellipticals — galaxies: evolution — galaxies: formation — galaxies: haloes

1 INTRODUCTION

In the standard theory (White & Rees 1978; Blumenthal et al. 1984; White & Frenk 1991), galaxy formation is a two-stage process. The gravitational instability of primordial density fluctuations forms dark matter haloes that merge hierarchically into larger and

larger structures. Galaxies grow within these haloes (i) by accreting gas that dissipates and falls to the centre of the gravitational potential wells of the dark matter and (ii) by merging with other galaxies after their haloes have become part of larger structures. These two paths explain why there are two galaxy morphological types: in the standard theory,

gas accretion is the mechanism that forms disc galaxies (i.e. spirals; Fall & Efstathiou 1980), while galaxy merging is the mechanism that forms elliptical galaxies (Toomre 1977; Mamon 1992).

In the present article, we wish to address the question of how galaxies acquired their present-day stellar mass. Was it mainly through mergers or through smooth gas accretion? Were the mergers principally *wet* mergers of gas-rich galaxies or *dry* mergers of gas-poor galaxies? How important are major mergers compared to more minor ones?

To answer these questions, one must first estimate the build-up of dark matter haloes, either through Monte-Carlo merger-trees (Lacey & Cole 1993; Somerville & Kolatt 1999; Neistein & Dekel 2008) or through cosmological N-body simulations, which also provide spatial information. If we assume that the position of a galaxy is tracked by the centre of mass of its halo, then the halo merger rate will also give us the rate at which galaxies merge. It is more difficult to compute the stellar masses of galaxies prior to merging, which determine the contribution from gas accretion, because they depend not only on the gas mass that accretes onto galaxies but also on feedback processes that eject gas from galaxies.

There are two approaches to deal with this complexity. Semi-analytic models (SAMs, Kauffmann et al. 1993; Cole et al. 1994; also Cattaneo et al. 2006; Bower et al. 2006; Croton et al. 2006; Somerville et al. 2008; Lo Faro et al. 2009; Neistein & Weinmann 2009, and references therein) use simple recipes to describe the physics of the baryons within haloes. However, even the simplest SAMs quickly reach considerable complexity and involve a large number of free parameters.

The halo occupation distribution (HOD) approach (Berlind & Weinberg 2002; Yang et al. 2009) does not make any assumption about the physics that govern the number (Berlind & Weinberg 2002), the luminosity (Yang et al. 2003) or the stellar mass (Yang et al. 2009) of galaxies within haloes. Instead, in the HOD approach, one computes the statistical distributions that these properties must have as a function of halo mass and redshift to reproduce the observational data (assuming that the properties of dark matter haloes, i.e. the mass function and clustering, are modelled correctly). However, HOD models cannot tell us how much of this mass comes from gas accretion and how much comes from mergers.

Our approach is intermediate between the two. By using a single simple equation, we parametrise the mass of stars formed after gas accretion as a function of halo mass and redshift, taking into account various feedback effects that quench gas accretion and subsequent star formation. We compute galaxy mergers by following dark matter substructures. When the latter are no longer resolved, we merge the galaxies on a dynamical friction timescale using a formula calibrated on cosmological hydrodynamic simulations (Jiang et al. 2008). This approach allows to separate growth via gas accretion and growth via mergers. We shall see that our model involves only four free parameters, and is thus much simpler than SAMs, including the SAM/HOD hybrid model proposed by Neistein & Weinmann (2009), who parametrised the dependence of the time derivatives of the masses of the stellar, cold and hot gas components of galaxies as a function of halo mass and redshift. At the same

time, our model has a much stronger physical basis than the HODs.

The structure of the article is as follows. In Section 2, we present the N-body simulation used to follow the gravitational evolution of the dark matter, and two simple formulae, one that expresses the timescale for orbital decay of unresolved subhaloes, and the other that expresses the stellar mass at the centre of each halo if galaxies grew only by gas accretion. In Section 3, we present our results for the relative importance of gas accretion and mergers as a function of galaxy mass. Section 4 discusses our results and summarises our conclusions.

2 THE GALAXY FORMATION MODEL

2.1 Gravitational evolution of the dark matter

The hierarchical formation and clustering of dark matter haloes is followed by means of a cosmological N-body simulation. The computational volume of the simulation presented here is a cube with side length $L = 50h^{-1}\text{Mpc}$ and periodic boundary conditions. The values of the cosmological parameters used to generate the initial conditions at redshift $z = 50$ by means of the Zel'dovich approximation (Efstathiou et al. 1985) and to run the simulation are those from the Wilkinson Microwave Anisotropy Probe's 5th-year analysis (WMAP5) combined with results from type Ia supernovae and baryonic acoustic oscillations (Komatsu et al. 2009): $\Omega_m = 0.279$, $\Omega_\Lambda = 0.721$, $\Omega_b = 0.046$, $h = 0.70$, $\sigma_8 = 0.817$ and $n_s = 0.96$. The simulation was run with the tree-PM code GADGET2 (Springel 2005) at a resolution of 512^3 particles. We saved the outputs at 101 timesteps equally spaced in time ($\Delta t = 92h^{-1}\text{Myr}$) from $z = 10$ to $z = 0$. The number of timesteps was chosen so that Δt is smaller than any merging timescale. The particle mass is $7.3 \times 10^7 h^{-1} M_\odot$.

The MPI version of the AMIGA halo finder, AHF (Knollmann & Knebe 2009), was used to identify haloes and sub-haloes in each of the saved outputs¹. AHF is an improvement of the MHF halo finder (Gill et al. 2004), which locates peaks in an adaptively smoothed density field as prospective halo centres. The local potential minima are computed for each of these density peaks and the gravitationally bound particles are determined. Only peaks with at least 20 bound particles are considered as haloes and retained for further analysis. Therefore, the minimum halo mass is $1.5 \times 10^9 h^{-1} M_\odot$ (corresponding to $v_{\text{circ}} = 15 \text{ km s}^{-1}$). Our halo finding algorithm automatically identifies haloes, sub-haloes, sub-sub-haloes, and so on (see Knollmann & Knebe 2009 for the details of the algorithm).

For each halo at epoch z , we compute the virial radius r_{vir} , which is the radius where the mean density drops below $\Delta(z)$ times the critical density of the Universe at redshift z . The threshold $\Delta(z)$ is computed using the spherical top-hat collapse model and is a function of both cosmological model and time (Nakamura 1996, cited in Kitayama & Suto 1996; Gross 1997; Bryan & Norman 1998). For the cosmology that we are using, $\Delta = 98$ at $z = 0$, i.e. the overdensity at the

¹ AHF can be downloaded from <http://popia.ft.uam.es/AMIGA>

virial radius is 352 times the present-day mean density of the Universe.

After each halo has been identified by AHF in this manner, we define sub-haloes to be haloes (defined with the same overdensity Δ) that lie within the virial region of a more massive halo, the so-called host halo, of mass $M_{\text{halo}}^{\text{host}}$. As sub-haloes are embedded within their host halo, their own density profile usually shows a characteristic upturn at the radius $r_t \lesssim r_{\text{vir}}$ where the density profile becomes dominated by the surrounding host halo². We use this truncation radius as the outer edge of the sub-halo. Halo and sub-halo properties (i.e. mass, density profile, velocity dispersion, rotation curve) are calculated using the gravitationally bound particles inside either the virial radius r_{vir} for a host halo or the truncation radius r_t for a sub-halo.

We build merger trees by cross-correlating haloes in consecutive simulation outputs. For this purpose, we use a tool that comes with the AHF package, called *MergerTree*. As the name suggests, it serves the purpose of identifying corresponding objects in a same simulation at different redshifts. We follow each halo (either host or sub-halo) identified at redshift $z = 0$ backwards in time. The direct progenitor at the previous redshift is the one that shares the greatest number of particles with the present halo *and* is closest to it in mass. The latter criterion is important for sub-haloes as all their particles are also part of the host halo, but there is normally a large gap between sub-halo and host halo masses.

In the study presented here, we walk along the tree starting at redshift $z = 10$ and moving toward $z = 0$. Sub-haloes are followed within the environment of their respective hosts until the point where AHF can no longer resolve them either because they have been tidally disrupted or because they have merged with their host (of course, many sub-haloes survive until $z = 0$). Section 2.2 below describes how we follow sub-haloes when we can no longer resolve them numerically.

2.2 Growth via galaxy mergers

We associate galaxies to the smallest resolved dark matter substructures. We say that two haloes have merged at the time t_m when a subhalo is no longer resolved (Fig. 1). With this definition, the merging of two dark matter haloes is a necessary but non-sufficient condition for the merging of their central galaxies because generally a sub-halo ceases to be resolved before reaching the centre of its host halo. Let t_{df} be the time the sub-halo takes to reach the centre after it is no longer resolved. The galaxy at the centre of the sub-halo has merged with the galaxy at the centre of the host halo if $t_m + t_{\text{df}} \leq t_0$, where t_0 is the age of the universe today.

To compute the time for the satellite’s orbit to decay to the centre, we use Chandrasekhar’s (1943) dynamical friction time, which can be written as

² The actual density profile of sub-haloes after the removal of the host’s background drops faster than for isolated haloes (e.g. Kazantzidis et al. 2004). Only when measured within the background still present shall we find the characteristic upturn used here to define the truncation radius r_t .

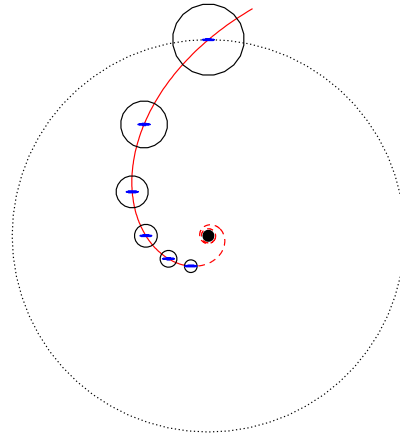


Figure 1. Sketch illustrating the merger of two haloes. Once the smaller halo penetrates the larger one, it becomes a sub-halo. Its orbit, shown by the *red curve*, decays by dynamical friction and its size, shown by the *circles*, is reduced by tidal stripping from the larger halo’s potential. The *solid part of the red curve* is followed directly by the N-body simulation, while the *dashed part* shows the trajectory that the sub-halo is expected to take after it is no longer resolved in the simulation. The duration of the motion along the dashed stretch of the red curve is computed analytically from Eqs.(1) and (3).

$$t_{\text{df}} = A \frac{r^2 v_{\text{circ}}}{GM_{\text{sat}} \ln \Lambda}, \quad (1)$$

(e.g. Binney & Tremaine 2008), where r is the sub-halo’s orbital radius at the time t_m when it ceases to be resolved, v_{circ} is the circular velocity at radius r , Λ is the so-called Coulomb logarithm, and A is a factor of order unity that depends on orbital eccentricity (see below).

Jiang et al. (2008) used high-resolution cosmological hydrodynamical simulations to show that, once a halo penetrates the virial sphere of a larger one (and thus becomes a sub-halo), the time it takes to fall to the centre of its parent halo is given by equation (1), where r and v_{circ} are measured at the virial radius r_{vir} of the host halo and where the Coulomb logarithm is $\ln \Lambda = \ln(1 + M_{\text{halo}}/M_{\text{sat}})$. We assume that for $r < r_{\text{vir}}$, the appropriate Coulomb logarithm is the one computed using

$$\Lambda = 1 + \frac{M_{\text{halo}}(r)}{M_{\text{sat}}}, \quad (2)$$

where $M_{\text{halo}}(r)$ is the halo mass enclosed within the sphere of radius r .

The normalisation A of the dynamical friction time is often chosen to be independent of the shape of the satellite’s orbit (e.g. 1.17 according to Binney & Tremaine 2008). But for given orbit apocenter, the time of orbital decay is expected to be shorter for satellites on radial orbits, which feel more dynamical friction as they reach the high density region near the centre of their halo. Jiang et al. calibrated this effect and found

$$A(\epsilon) = 1.17 (0.94 \epsilon^{0.6} + 0.6), \quad (3)$$

where $\epsilon = J/J_{\text{circ}}(E)$ is the orbital circularity, that is, the ratio of angular momentum to that of a circular orbit of the

same energy ($\epsilon = 0$ for a radial orbit and $\epsilon = 1$ for a circular orbit). Jiang et al.'s parametrisation of the Coulomb logarithm and normalisation of the orbital decay time implicitly take into account the greater concentration of baryons with respect to the dark matter and already includes the effects of tidal stripping on the dynamical friction time.

The value of ϵ is computed as follows. The radial coordinate r , the orbital speed v , and the radial and tangential velocities v_r and $v_t = \sqrt{v^2 - v_r^2}$ of the sub-halo with respect to the centre of mass of the host halo are extracted from the N-body simulation at the last timestep when the sub-halo is resolved. We compute the sub-halo's angular momentum and energy per unit mass. They are, respectively, $J = r v_t$ and $E = 1/2 M v^2 + \phi(r)$, where $\phi(r)$ is the gravitational potential of the host halo that we compute assuming an NFW model (Navarro et al. 1996). This requires to know the halo concentration. The latter could be evaluated directly from the particle distribution but this may lead to noise, particularly in low-mass haloes, which contain fewer particles. Instead, we use the most recent determination of the concentration-mass relation for regular haloes in Λ CDM simulations with WMAP-5th year cosmological parameters (Macciò et al. 2008): $c = 6.1 (M_{\text{halo}}/10^{14} h M_{\odot})^{-0.094}$. With this assumption we compute $J_{\text{circ}}(E)$ by solving the equation $E = 1/2 v_{\text{circ}}^2 + \phi(r)$ for r where the squared circular velocity is $v_{\text{circ}}^2 = G M_{\text{halo}}^{\text{host}}(r)/r$, and where $M_{\text{halo}}^{\text{host}}(r)$ is also computed with the NFW model. This equation has a solution for $E < 0$. When $E \geq 0$, the sub-structure is not gravitationally bound to the host, so the satellite and the central galaxy do not merge.

In our analysis, the galaxy merging history is determined fully and solely by the underlying evolution of the dark matter component. It does not depend on the efficiency with which gas dissipates, sinks to the centre and makes stars. This is why we have discussed galaxy mergers immediately after presenting the N-body simulation. The processes that determine the growth of luminous galaxies via accretion within dark matter haloes are considered in the following subsection.

2.3 Growth via gas accretion

The model to compute $m_{\text{stars}}^{\text{accr}}$ as a function of M_{halo} , that is, the baryonic mass that is expected to have made stars in a halo of mass M_{halo} , is an improvement of the one introduced by Cattaneo (2001). Despite its simplicity, this model was shown to be in reasonable agreement with the galaxy luminosity function and the cosmic evolution of the star formation rate (SFR) density. The physics of galaxy formation enter the model in three ways: cosmic reionisation suppresses gas accretion and star formation in haloes below a minimum circular velocity v_{reion} , stellar feedback mitigates star formation in haloes below a characteristic circular velocity v_{SN} , and gravitational shock heating coupled to black hole feedback suppresses gas accretion and star formation above a critical halo mass of M_{shock} . We now explain the details of how these processes are modelled.

Shock heating and AGN feedback. When the halo mass is above a critical mass of $M_{\text{shock}} \sim 10^{12} M_{\odot}$, the infalling gas is shock heated and ceases to accrete onto the galaxy (Birnboim & Dekel 2003; Dekel & Birnboim 2006), while active galactic nuclei couple to the hot gas preventing

it from cooling down again (Silk & Rees 1998; Croton et al. 2006; Cattaneo et al. 2009, and references therein). Following Cattaneo (2001), we model this effect by assuming that the accreted mass is, to first order,

$$m_{\text{accr}}^{(1)} = \frac{f_b M_{\text{halo}}}{1 + M_{\text{halo}}/M_{\text{shock}}} \quad (4)$$

(for $v_{\text{circ}} \gg v_{\text{reion}}$). In other words, $m_{\text{accr}}^{(1)} \simeq f_b M_{\text{halo}}$ when $M_{\text{halo}} \ll M_{\text{shock}}$, while $m_{\text{accr}}^{(1)} \simeq f_b M_{\text{shock}}$ when $M_{\text{halo}} \gg M_{\text{shock}}$. In the latter case, the galaxy mass grows very slowly with increasing halo mass (except for the effects of mergers, which are not considered in the calculation of the accreted mass).

Reionisation. Heating by the photoionising UV background raises the entropy of the gas and suppresses the concentration of baryons in shallow potential wells (Blanchard, Valls-Gabaud, & Mamon 1992; Efsthathiou 1992; Gnedin 2000; Kravtsov, Gnedin, & Klypin 2004). Here we take a phenomenological approach and model the effects of photoionisation heating by introducing a lower circular velocity cut-off at $v_{\text{circ}} \sim v_{\text{reion}}$ that mimicks the shutoff of gas infall when $T_{\text{vir}} < T_{\text{IGM}}$ (Blanchard et al. 1992; Thoul & Weinberg 1996). Cosmological hydrodynamical simulations give conflicting answers on the temperature of the intergalactic medium (IGM) in the intermediate density regions outside the virial radius, from which gas should fall in (McQuinn et al. 2009, and references therein). We assume that this IGM temperature does not vary with redshift at $z \gtrsim z_{\text{reion}} > 10$ ($z \simeq 10$ is where our calculations start), which is in rough agreement with the simulations (McQuinn et al. 2009, and references therein). We also suppose that the mass m_{accr} that can flow to the centre in a halo of mass M_{halo} is suppressed with respect to the first-order accreted mass by a factor of $1 - (v_{\text{reion}}/v_{\text{circ}})^2$ at $v_{\text{circ}} \geq v_{\text{reion}}$, so that:

$$m_{\text{accr}} = \left[1 - \left(\frac{v_{\text{reion}}}{v_{\text{circ}}} \right)^2 \right] m_{\text{accr}}^{(1)}. \quad (5)$$

At $v_{\text{circ}} < v_{\text{reion}}$ the suppression is total ($m_{\text{accr}} = 0$). This extreme approximation is *ad hoc*, but it is not unreasonable given the high mass-to-light ratios measured in low-mass objects. The sharp suppression of gas infall has been found in spherical modelling of gas infall by Thoul & Weinberg (1996).

Supernovae. When the circular velocity becomes larger than v_{reion} , the gas starts flowing to the centre and making stars, which feed energy back to the interstellar medium mainly via type II supernova explosions. The energy fed back to the interstellar medium is proportional to the stellar mass formed. A fraction of this energy is used to drive an outflow. For a given wind kinetic energy, $1/2 m_{\text{wind}} v_{\text{wind}}^2$, the wind mass m_{wind} is maximum when the wind speed, v_{wind} , is minimum. However, the wind speed cannot be lower than the escape velocity, which is proportional to the circular velocity v_{circ} , because otherwise the gas would not flow out. The maximum outflow condition implies that $m_{\text{wind}} = (v_{\text{SN}}/v_{\text{circ}})^2 m_{\text{stars}}^{\text{accr}}$ (Dekel & Silk 1986), where v_{SN}^2 is a proportionality constant, the value of which is to be determined by fitting the galaxy mass function and is physically related to the supernova energy that goes into wind kinetic energy. We also require that $m_{\text{wind}} + m_{\text{stars}}^{\text{accr}} = m_{\text{accr}}$. This is the same as saying that, eventually, all the gas ac-

creted onto a galaxy is either ejected or forms stars. This assumption is crude because galaxies do not turn all the accreted gas instantaneously into stars. However, even in spiral galaxies, typical gas fractions (cold gas divided by cold gas plus stars) rarely exceed $\sim 10 - 20\%$, so the error on the galaxy stellar mass that one makes by assuming that the entire galaxy mass is in stars is consistent with the other uncertainties of our model. When we substitute $m_{\text{wind}} = (v_{\text{SN}}/v_{\text{circ}})^2 m_{\text{stars}}^{\text{accr}}$ into $m_{\text{wind}} + m_{\text{stars}}^{\text{accr}} = m_{\text{accr}}$, we find

$$m_{\text{stars}}^{\text{accr}} = \frac{v_{\text{circ}}^2}{v_{\text{circ}}^2 + v_{\text{SN}}^2} m_{\text{accr}}. \quad (6)$$

By putting together Eqs. (4), (5), and (6), we can write a simple but physically motivated equation for the stellar mass of the central galaxy of a halo of mass M_{halo} in the absence of merging:

$$m_{\text{stars}}^{\text{accr}} \sim \frac{v_{\text{circ}}^2 - v_{\text{reion}}^2}{v_{\text{circ}}^2 + v_{\text{SN}}^2} \frac{f_{\text{b}} M_{\text{halo}}}{1 + M_{\text{halo}}/M_{\text{shock}}}, \quad (7)$$

where

$$\begin{aligned} v_{\text{circ}} &\equiv v_{\text{circ}}(M_{\text{halo}}, z) \\ &= \left[\frac{\Delta(z)}{2} \right]^{1/6} [GH(z)]^{1/3} M_{\text{halo}}^{1/3}. \end{aligned} \quad (8)$$

At each timestep, the galaxy stellar mass is assigned according to equations (7) and (8), unless this produces a lower stellar mass than at the previous timestep. Similar simple toy models were independently constructed by D. Croton (private communication) and by A. Dekel (private communication) although in their models the low-mass cut-off does not depend on redshift.

2.4 Tidal stripping

The dynamical friction time given by eqs. (1), (2) and (3), which was calibrated by Jiang et al. (2008) on hydrodynamical cosmological simulations, implicitly incorporates the effects of tides, which strip the secondaries to lower masses as they orbit through the primary, on the dynamical friction time. However, knowledge of the stellar mass at a given time is necessary to compare to the observed galaxy mass function, so we need to estimate the time evolution of the stellar mass caused by tidal stripping.

Tidal forces are known to strip galaxy haloes very efficiently once they penetrate larger ones (e.g. Ghigna et al. 1998), and each pericentric passage generates more mass loss (Hayashi et al. 2003). But tides also affect, to a lesser extent, the more bound stellar material. For example, Klimentowski et al. (2009) ran simulations of a low-mass high-resolution spiral galaxy around the fixed potential of the Milky Way and found that over 5 orbits, while the dark matter mass was reduced by a factor 100, the stellar mass was reduced by a factor 10, meaning that a fraction of $\eta_{\text{strip}} = 1 - (1/10)^{1/5} = 0.37$ of the stellar mass was lost at every pericentric passage. This tidally stripped stellar mass should form what is known as the stellar halo in the case of a galaxy and the intracluster light in the case of a cluster.

According to the simulations of Klimentowski et al., the mean mass loss η_{strip} is roughly constant for every pericentric passage, so the importance of tidal stripping depends on

Table 1. Best fit parameters corresponding to the full model in Figure 2.

v_{reion}	40 km s ⁻¹
v_{SN}	120 km s ⁻¹
M_{shock}	$8 \times 10^{11} h^{-1} M_{\odot}$
η_{strip}	0.4

the number of orbital revolutions that a galaxy makes from when its orbit starts decaying to when either the galaxy merges with the central galaxy of its parent halo or the simulation ends. In the former case, the total time span during which a galaxy is stripped is given by the time it takes to decay by dynamical friction from the virial radius to the centre (Eq. 1 with r and v_{circ} taken at the virial radius). Taking $t_{\text{orb}} \sim 2\pi r/v_{\text{circ}}$ for the orbital time, we find

$$\frac{t_{\text{df}}}{t_{\text{orb}}} = \frac{A(\epsilon)}{2\pi} \frac{r_{\text{vir}} v_{\text{circ}}^2}{GM_{\text{sat}} \ln \Lambda} = \frac{A(\epsilon)}{2\pi} \frac{M_{\text{halo}}^{\text{host}}/M_{\text{sat}}}{\ln(1 + M_{\text{halo}}^{\text{host}}/M_{\text{sat}})}. \quad (9)$$

The calibration of the dynamical friction time $A(\epsilon)$ is computed using the formula in Jiang et al. (2008), which fits the results of SPH simulations and accounts for the tidal stripping of sub-structures. Eq. (9) implies that, for a fixed value of η_{strip} , the importance of tidal stripping increases with $M_{\text{halo}}^{\text{host}}/M_{\text{sat}}$.

In conclusion, our model for $m_{\text{stars}}^{\text{accr}}$ depends on three free parameters only, v_{reion} , v_{SN} , and M_{shock} , while there are no free parameters in the calculation of the halo and thus galaxy merger rate. We have a fourth parameter, η_{strip} , which affects the final galaxy masses by controlling the efficiency of tidal stripping, but we are about to see that this parameter has comparatively little bearing on our results.

3 RESULTS

3.1 Best fit model and effects of physical processes

We present the results of seven models, which correspond to different choices of v_{reion} , v_{SN} , M_{shock} , and η_{strip} . We start from the model that fits best the mass function by Bell et al. (2003) and then consider how the predictions vary when the assumptions are changed.

The stellar masses used by Bell et al. (2003) to compute the mass function from observational data depend on the Hubble constant used to compute galaxy luminosities and on the stellar initial mass function (IMF). The masses inferred from observed luminosities scale as h^{-2} while simulated masses scale as h^{-1} . As it is not possible to make the comparison between model and observations completely independent of h , we convert the observationally determined masses in units of $h^{-1} M_{\odot}$ by assuming $h = 0.7$. Bell et al. (2003) compute the stellar mass function using a diet Salpeter IMF (Bell & de Jong 2001). To convert to a Salpeter (1955) or a Kroupa (2002) IMF, one should add a correction of +0.15 and -0.1 dex, respectively (see Bell et al. (2003)).

The model that we have described in Section 2 is a good fit to the Bell et al. (2003) mass function at $10^{8.7} M_{\odot} < m_{\text{stars}} h < 10^{11.6} M_{\odot}$ for the parameter combination in Ta-

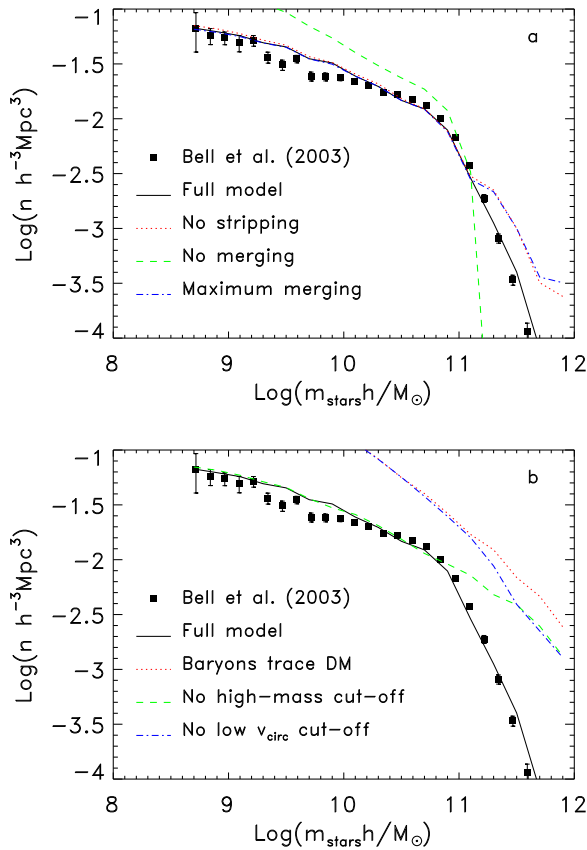


Figure 2. Stellar mass function of galaxies at $z = 0$. The *filled squares* show the galaxy mass function determined observationally by Bell et al. (2003). The *solid line* shows our best fit model (the ‘full’ model, with parameter values listed in Table 1). The fit assumes $h = 0.7$ because observationally inferred masses scale as h^{-2} . (a) Variations of the stellar mass function for different assumptions on merging and stripping: best-fit full model (*black solid line*), no tidal stripping ($\eta_{\text{strip}} = 0$, *red dotted line*), no mergers at all (*green dashed line*), and maximum merging (*blue dash-dotted line*). (b) Variations of the stellar mass function for different assumptions on the baryonic physics: best-fit full model (*black solid line*), baryons trace dark matter ($m_{\text{stars}}^{\text{accr}} = f_b M_{\text{halo}}$, *red dotted line*), no high-mass cutoff ($M_{\text{shock}} \rightarrow \infty$, *green dashed line*), and no low circular velocity cutoff ($v_{\text{SN}} = v_{\text{reion}} = 0$, *blue dash-dotted line*). In both panels, all variations start from the best-fit parameters of the full model except for the fact that we use $\eta_{\text{strip}} = 0$ in all models apart from the full one.

ble 1 (Figure 2, full model). Different determinations of the stellar mass function (e.g. Baldry et al. 2008; Yang et al. 2009) would give different best fit parameters. As the galaxy mass function depends on the assumed stellar IMF, so do our best-fit parameters. However, the conclusions of our article are robust to these changes and they do not depend on the precise values of the model parameters. We also note that $v_{\text{SN}} = 120 \text{ km s}^{-1}$ is close to the value of 100 km s^{-1} derived by Dekel & Silk (1986). It implies a supernova efficiency of $\sim 1\%$ if there is one 10^{52} erg supernova every $100 M_{\odot}$ of star formation and the escape speed is $\sqrt{3} v_{\text{circ}}$, that is, the required wind kinetic energy is $\sim 1\%$ of the supernova energy.

The incorporation of η_{strip} reduces the stellar masses of satellite galaxies at each timestep. Comparison with the

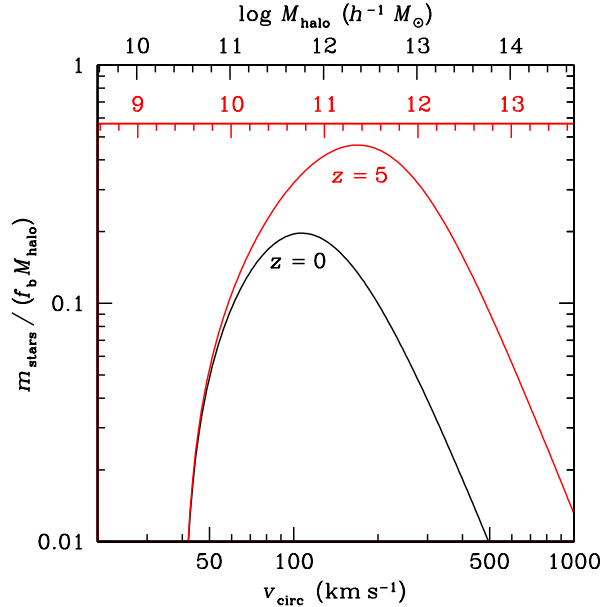


Figure 3. Star formation efficiency versus halo circular velocity and mass at two different epochs for the best-fit parameters of Table 1. The *upper (black)* mass scale is for $z = 0$, while the *lower (red)* mass scale is for $z = 5$.

case $\eta_{\text{strip}} = 0$ (Figure 2a, dotted line) shows that this effect is negligible at $m_{\text{stars}} \lesssim 10^{11} h^{-1} M_{\odot}$, where most galaxies are central. Tidal stripping is, however, important at higher masses, where the galaxy mass function is predicted to be shifted toward high masses by ~ 0.2 dex in mass compared to the Bell et al. (2003) mass function if satellites are not stripped of part of their mass before they merge into the galaxies that populate this part of the mass function. This discrepancy may largely be due to systematic measurement errors in the data, since many massive ellipticals extend outside the photometric aperture used to measure their luminosities. Lauer et al. (2007) find errors of up to a magnitude in the SDSS luminosities of such galaxies and these are the same data that anchor the top end of the Bell et al. mass function in Figure 2. We shall elaborate on this in the Discussion (Section 4).

Figure 3 illustrates how the efficiency with which halo mass growth results in stellar mass growth depends on halo mass at two different redshifts for the best-fit parameters of Table 1. The star formation efficiency is maximum at $M_{\text{halo}} \sim 10^{11} - 10^{12} h^{-1} M_{\odot}$, decreasing sharply at lower masses and more mildly at higher masses. Figure 3 shows that in a $z = 0$ halo, $< 20\%$ of the baryonic mass is expected to be in stars. The fraction of baryons that may be locked up in stars can reach 50% at high redshift, where feedback is less important because the circular velocity thresholds of equation (7) correspond to lower mass thresholds (eq. [8], noting that $\Delta(z)$ and especially $H(z)$ increase with z).

Assuming that every halo merger immediately results in a galaxy merger causes the most massive galaxies to grow even larger (dash-dotted line in Figure 2a) but the difference between the dash-dotted line and the dotted line is fairly minor suggesting that most halo mergers do result in galaxy mergers. The difference between the two curves in the high-

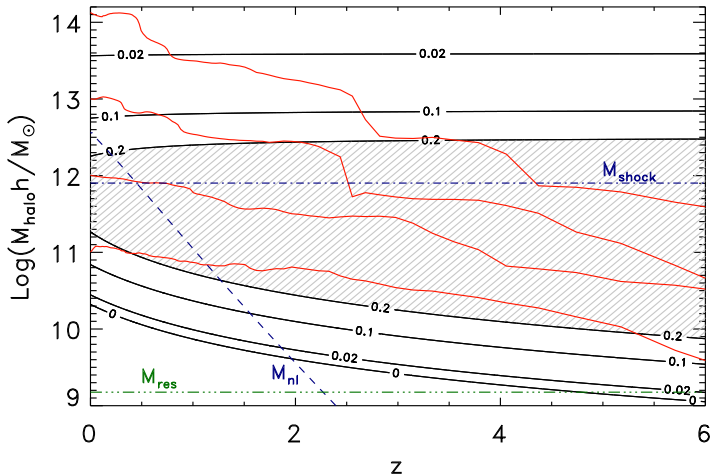


Figure 4. Growth of halo mass and efficiency of star formation. The contours show the efficiency of star formation, $m_{\text{stars}}^{\text{accr}}/(f_b M_{\text{halo}})$, as a function of redshift and halo mass, for the set of parameters that fit best the galaxy mass function (Table 1). The horizontal dash-dotted line shows the critical halo mass for shock heating, $M_{\text{halo}} = M_{\text{shock}}$. Baryons make stars efficiently only in the horizontal band of the diagram shown by the shaded region. The red irregular lines show the mass growth of four haloes, whose present masses are about 10^{11} , 10^{12} , 10^{13} and $10^{14} h^{-1} M_{\odot}$. They are backwards tracks for the most massive progenitors. The diagonal dashed line shows the characteristic mass scale M_{nl} on which density fluctuations become non-linear at redshift z , i.e. where $\sigma(M_{\text{nl}}, z) = 1.68$. The horizontal green line shows the mass resolution $M_{\text{res}} = 1.5 \times 10^9 h^{-1} M_{\odot}$ of the N-body simulation.

est mass bin disappears if the dash-dotted line is computed not for all halo mergers, but for those of bound halo-satellite systems.

The dashed line in Figure 2a corresponds to the extreme opposite assumption that whenever a new halo appears a new galaxy is created but there are no galaxy mergers at all. This assumption predicts too many low-mass galaxies and too few high-mass galaxies with respect to the observations.

Both the dotted line and the dash-dotted line in Figure 2a assume models without tidal stripping (so does the dashed line). In both cases the cosmic stellar mass density obtained by integrating the stellar mass function over all masses exceeds the observational value inferred from the Bell et al. (2003) mass function. This suggests that stripping is necessary, since changing the merging rate does not affect the cosmic stellar mass density.

Having seen how the mass function depends on the capture and the probable stripping of satellites, we now examine how it depends on our assumptions on the quiescent growth of galaxies in isolated haloes (Figure 2b). We compare the full model with three unrealistic simpler models, which are, however, useful for illustrative purposes. They are: i) a model in which the stellar mass grows proportionally to the mass of the dark matter ($m_{\text{stars}}^{\text{accr}} = f_b M_{\text{halo}}$; dotted line); ii) a model with the term in v_{circ} but without the cutoff at high masses (dashed line); and iii) a model with the cutoff at high masses but not the term in v_{circ} (dash-dotted line).

Figure 2b illustrates the well known fact that supernova

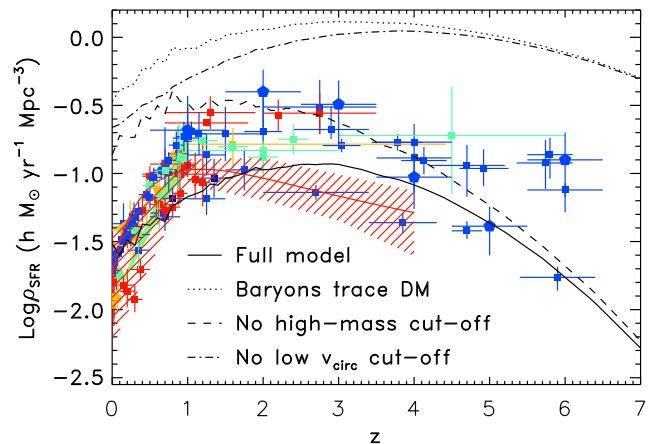


Figure 5. The evolution of the cosmic SFR density with redshift in the Universe (points with error bars and hatched region) and in our model (black solid line). The blue squares are UV data Giavalisco et al. (2004); Wilson et al. (2002); Massarotti et al. (2001); Sullivan et al. (2000); Steidel et al. (1999); Cowie et al. (1999); Treyer et al. (1998); Connolly et al. (1997); Baldry et al. (2005); Schiminovich et al. (2005); Wolf et al. (2003); Arnouts et al. (2005); Bouwens et al. (2003); Bouwens (2006); Bunker et al. (2004); Ouchi et al. (2004). The blue pentagons are Hubble Ultra Deep Field estimates (Thompson et al. 2006). The red squares are $H\alpha$, $H\beta$ and OII data (Hanish et al. 2006; Pérez-González et al. 2003; Tresse et al. 2002; Hopkins et al. 2000; Moorwood et al. 2000; Sullivan et al. 2000; Glazebrook et al. 1999; Yan et al. 1999; Tresse & Maddox 1998; Gallego et al. 1995; Pettini et al. 1998; Teplitz et al. 2003; Gallego et al. 2002; Hogg et al. 1998; Hammer et al. 1997). The orange squares are 1.4 GHz data (Mauch & Sadler 2007; Condon et al. 2002; Sadler et al. 2002; Serjeant et al. 2002; Machalski & Godlowski 2000; Haarsma et al. 2000; Condon 1989). The orange pentagon at $z \simeq 0.24$ is X-ray data (Georgakakis et al. 2003). The green squares are infrared (Pérez-González et al. 2005; Flores et al. 1999) and sub-mm (Barger et al. 2000) data. The green hatched region is the far infrared ($24 \mu\text{m}$) SFR history from Le Floc’h et al. (2005). The data shown here are all rescaled for a Salpeter stellar initial mass function and $h = 0.7$. Most of them were taken from the compilations in Hopkins (2004) and Hopkins & Beacom (2006). The red curve, $\dot{\rho}_{\text{stars}} = (0.014 + 0.11z) h/[1 + (z/1.4)^{2.2}](h/0.7) M_{\odot} \text{Mpc}^{-3}$, is the cosmic SFR derived by Wilkins et al. (2008) by taking the derivative of the cosmic stellar mass density, i.e. from the variation of the observed stellar mass functions with z rather than from star formation rate measurements. The red shaded area shows the margins of uncertainty around the red curve. All observational data have been corrected (-0.15 dex) to the diet Salpeter IMF assumed by Bell et al. (2003), on whose mass function we have calibrated our model.

and reionisation feedback processes are essential to reconcile the observed galaxy mass function with the halo mass function of a cold dark matter Universe (compare the solid line and the dash-dotted line). The suppression of star formation at $M_{\text{halo}} > M_{\text{shock}}$ is necessary to reproduce the break in the galaxy stellar mass function at $\sim 10^{11} M_{\odot}$ (compare the solid line and the dashed line). It is the combination of these low and high mass cut-offs that allows the best fit model to reproduce the normalisation and the characteristic break of the galaxy stellar mass function. Figure 2b shows

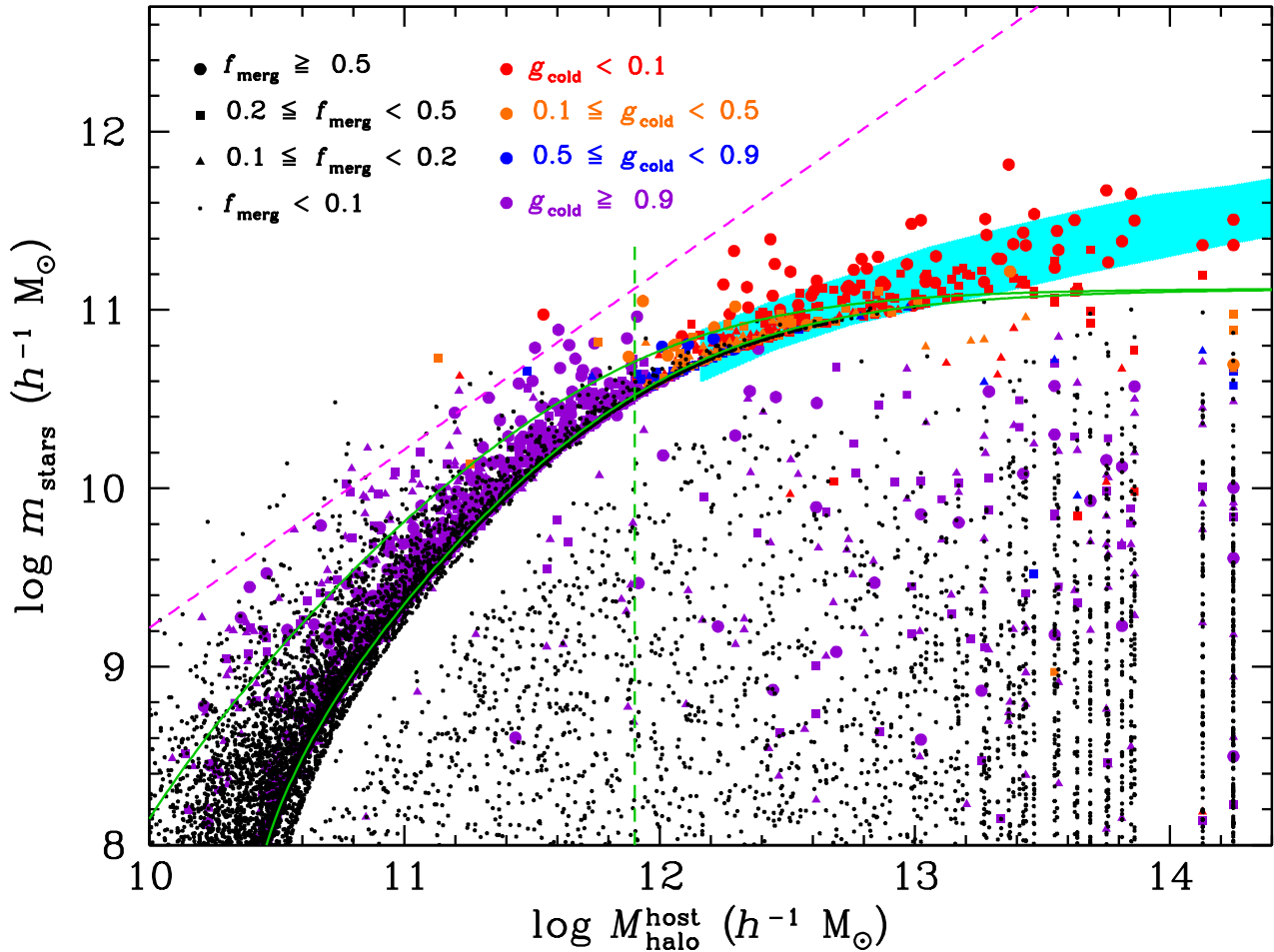


Figure 6. Galaxy stellar mass vs. host halo mass at $z = 0$ for the set of parameters that fit best the galaxy stellar mass function. Each point is a galaxy. The symbol sizes and colours vary with the fraction of mass acquired in mergers, and the fraction g_{cold} of this mass acquired by cold-mode mergers (where the masses of the haloes of the two merging galaxies are both below M_{shock}), respectively, according to the legend. The *vertical green line* corresponds to $M_{\text{halo}} = M_{\text{shock}}$, while the *oblique magenta line* indicates $m_{\text{stars}} = f_b M_{\text{halo}}$. The green curves show the stellar masses of galaxies acquired through the accretion channel (eq. [7] with best-fit parameters from Table 1) at $z = 0$ (*lower*) and $z = 3$ (*upper curve*). The *shaded cyan region* corresponds to the observations from the SDSS (Yang et al. 2009), shifted upwards by $\log_{10}(1/h) = 0.15$ to take into account the different h -dependence of the observed stellar masses ($\propto h^{-2}$) and the stellar masses computed from eq. (7) ($\propto h^{-1}$) and by an additional factor of $+0.1$ dex to pass from the Kroupa IMF assumed by Yang et al. (2009) to the diet Salpeter IMF assumed by Bell et al. (2003), on whose mass function we have calibrated our model.

that the low v_{circ} cut-off is important not only for the low-mass end but also for the high-mass end of the galaxy mass function because the high-mass cut-off alone is not enough if the building blocks of giant ellipticals have been allowed to grow in an uncontrolled fashion before crossing the critical mass. This result agrees with what N. Katz finds from hydrodynamic simulations (private communication). We also find that the quenching of high mass galaxies by shock heating is much more effective than the reduction of their masses by tidal stripping, as it can be seen by comparing Figs. 2a (red dotted curve) and 2b (green dashed curve).

Figure 4 shows how this combination of processes quenching star formation works during the growth of a dark matter halo. The contours show $m_{\text{stars}}^{\text{accr}}/(f_b M_{\text{halo}})$ as a function of halo mass and redshift. They have been plotted for the parameter set that gives the best fit to the galaxy mass function (Table 1). The term in v_{circ} in

Eq. (7) suppresses galaxy formation in low-mass haloes, while the cut-off at M_{shock} suppresses galaxy formation in high-mass haloes. The result is a *galaxy formation zone* at $10^{10} M_{\odot} \lesssim M_{\text{halo}} h \lesssim 10^{12.5} M_{\odot}$. Galaxy formation begins and ends when a halo moves in and out of the galaxy formation zone, respectively. The four red curves in Figure 4 show the mass growth with redshift of four haloes whose final masses at $z = 0$ are roughly 10^{11} , 10^{12} , 10^{13} and $10^{14} h^{-1} M_{\odot}$. The haloes that are more massive enter and exit the galaxy formation zone at an earlier epoch. Since the most massive haloes contain the most massive galaxies, this explains why the most massive galaxies contain the oldest stellar populations (*archaeological downsizing*, Cattaneo et al. 2008).

The dashed curve in Figure 4 shows the characteristic mass M_{nl} of density fluctuations that become non-linear at redshift z , i.e. the characteristic mass scale on which the

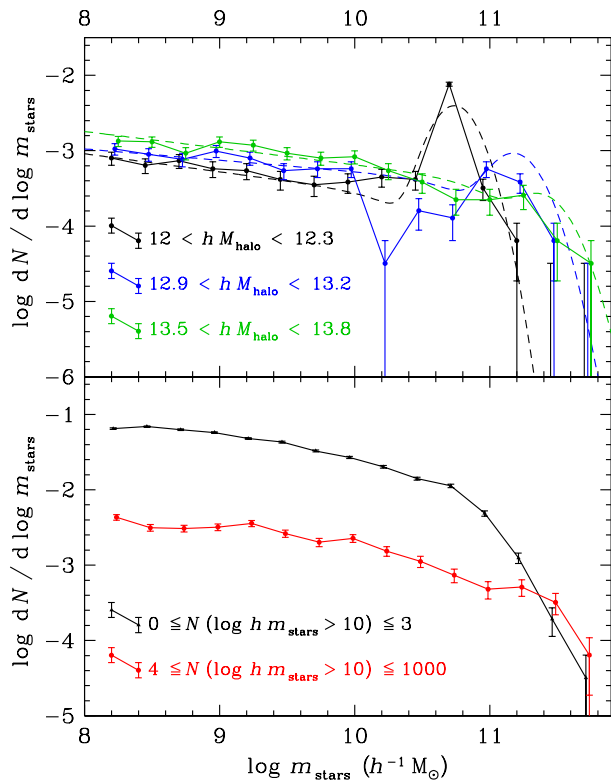


Figure 7. The galaxy stellar mass function at $z = 0$ split by environment, defined by host halo mass (*top*) or group richness (number of companions with $m_{\text{stars}} > 10^{10} M_{\odot}/h$ in the same host halo, *bottom*). The dashed curves in the top panel show the condition mass function fits to the SDSS data by Yang et al. (2009). The same h and IMF corrections as in Fig. 6 apply.

cosmic variance of linearly extrapolated primordial density fluctuations is equal to $\delta_c \simeq 1.68$ at redshift z . Here δ_c is the density contrast of a top hat fluctuation that the linear theory predicts at the time when the fluctuation actually collapses. The value of δ_c depends very weakly on Ω_m and Ω_{Λ} . The redshifts at which M_{nl} comes in and out of the galaxy formation zone mark the beginning and the end of the main epoch of galaxy formation in the Universe.

Figure 5 shows the evolution of the cosmic SFR density that our best-fit model predicts if we assume that the star formation timescale is always short compared to the age of the Universe, so that gas makes stars at the rate at which it accretes onto galaxies. The agreement between our best-fit model and the data (especially the more comparable run of differential stellar mass function of Wilkins et al. 2008) is reasonable given how simple our model is³. We shall return to this point in Sect. 4.

³ The discrepancy in Figure 5 between the directly measured SFR densities (symbols with error bars) and the evolution of the SFR density computed from the time derivative of the stellar mass function (red curve and shaded area) is an open observational problem.

3.2 Central and satellite galaxies: the role of the environment

Figure 6 provides a deeper insight of what happens inside our model. We have plotted all our simulated galaxies in an m_{stars} vs. $M_{\text{halo}}^{\text{host}}$ diagram, where $M_{\text{halo}}^{\text{host}}$ is the mass of the largest halo in which a galaxy is contained (so that if a small galaxy is located near a larger one, itself within a group of galaxies, the host halo is that of the group and not that of the larger galaxy). The symbol with which a galaxy is plotted has been sized and colour-coded according to the value of f_{merg} (size) and the fraction, g_{cold} , of the mass acquired by mergers that was acquired in cold-mode mergers. Only the best fit model, corresponding to the solid line in Figure 2, has been shown.

We clearly see two galaxy populations separated by an empty zone: a population of central galaxies (galaxies for which $M_{\text{halo}}^{\text{host}} = M_{\text{halo}}$), which form a curved band in the $m_{\text{stars}} - M_{\text{halo}}^{\text{host}}$ plane, roughly following the stellar masses predicted from the accretion channel (eq. [7] and green curves of Figure 6), and a population of satellite galaxies ($M_{\text{halo}} < M_{\text{halo}}^{\text{host}}$), which are scattered over a broad area of the diagram lying below the central galaxy relation.

Central galaxies with $f_{\text{merg}} \lesssim 0.1$ tend to accumulate in a narrow zone of the $m_{\text{stars}} - M_{\text{halo}}^{\text{host}}$ diagram, which appears as a black curve of points, and corresponds to the present-day $m_{\text{stars}} - M_{\text{halo}}$ relation (lower green curve) given by Eq. (7). Its broadness is due to the higher value, for given $M_{\text{halo}}^{\text{host}}$, of v_{circ} and therefore m_{stars} at higher redshifts, as can be seen from the two green curves in Figure 6. Galaxies that lie well above the critical $z = 0$ curve either live in haloes that have lost mass due to tidal stripping (dots and triangles) or are galaxies that have grown above the relation by mergers (filled circles).

The mass gap between central and satellite galaxies is also evident in the analysis of SDSS galaxies by Yang et al. (2008) (their Fig. 4). In fact, the $m_{\text{stars}} - M_{\text{halo}}^{\text{host}}$ relation predicted for the central galaxies of groups and clusters in Figure 6 is highly consistent with that found in the SDSS shown in Fig. 4 of Yang et al. (2009) (shaded region in Fig. 6). The small differences between our results and theirs are consistent with the different observational determinations of the galaxy mass function that we have used to constrain our models, since the Yang et al. mass function is shifted by ~ 0.1 dex in mass towards higher masses with respect the Bell et al. mass function at $m_{\text{stars}} > 10^{11} M_{\odot}$ even after correcting for the different stellar initial mass functions assumed by these authors. Moreover, Yang et al. (2009), too, find a gap between the stellar masses of central and satellite galaxies at a given host halo mass.

Figure 7a shows how different environments contribute to the galaxy stellar mass function at $z = 0$. The mass function in haloes with $10^{12} M_{\odot} < h M_{\text{halo}} < 10^{12.3} M_{\odot}$ contains a strong peak at $m_{\text{stars}} \sim 10^{10.7} h^{-1} M_{\odot}$, the characteristic mass of the central galaxy of a halo in that mass range (Figure 6, black curve). The contribution of its satellites to the galaxy mass function is at least an order of magnitude smaller than that of the galaxy. In a halo with $10^{12.9} M_{\odot} < h M_{\text{halo}} < 10^{13.2} M_{\odot}$, the relative contribution of satellite galaxies is higher but we still see a clear gap between central and satellite galaxies at $m_{\text{stars}} \sim 10^{10.4} h^{-1} M_{\odot}$, while the central galaxy peak has moved up to

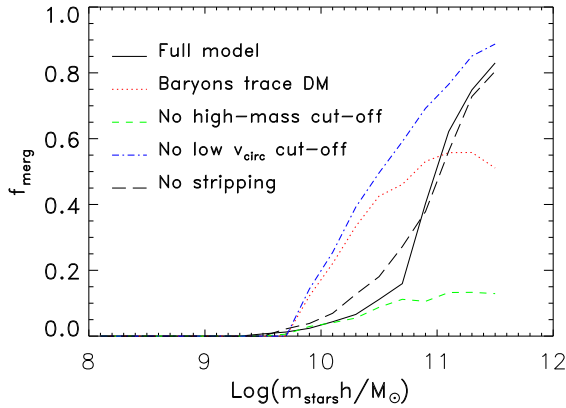


Figure 8. Median fraction of the $z = 0$ galaxy mass acquired via mergers rather than via gas accretion for various models: best-fit full model (*solid line*), baryons trace dark matter ($m_{\text{stars}}^{\text{accr}} = f_b M_{\text{halo}}$, *dotted line*), no high-mass cutoff ($M_{\text{shock}} \rightarrow \infty$, *short-dashed line*), no low circular velocity cutoff ($v_{\text{SN}} = v_{\text{reion}} = 0$, *dash-dotted line*), and no tidal stripping ($\eta_{\text{strip}} = 0$, *long-dashed line*).

$m_{\text{stars}} \sim 10^{11.1} h^{-1} M_{\odot}$ (blue curve). The peak of the green curve is at a lower number density than the peak of the blue curve, because there are less central galaxies of haloes with $10^{12.9} M_{\odot} < M_{\text{halo}} h < 10^{13.2} M_{\odot}$ than there are central galaxies of haloes with $10^{12} M_{\odot} < M_{\text{halo}} h < 10^{12.3} M_{\odot}$. At $10^{13.5} M_{\odot} < M_{\text{halo}} h < 10^{13.8} M_{\odot}$, the satellite population has become so numerous and the central galaxy peak has moved down so much that the gap is no longer visible (green curve). Thus, the more massive the halo, the more important the satellite population.

A similar behaviour is also seen in the analysis of SDSS galaxies by Yang et al. (2009), with gaps and peaks occurring at very similar values of m_{stars} (we used the same narrow bins of halo mass as they did for a better comparison).

For observers, it is easier to define the environment of a given galaxy with the number of companions above a luminosity limit than by its halo mass. For this reason, in Figure 7b we show how the galaxy stellar mass function differs between rich and poor systems, where rich and poor are defined by having respectively less than four or at least four companions with $m_{\text{stars}} > 10^{10} h^{-1} M_{\odot}$. Since we use two wide bins of richness in Figure 7b, we cannot see peaks as we did in Figure 7a. However, there is an important difference between the mass functions of poor and rich systems: poor systems display a strong lack in massive galaxies relative to richer systems. In contrast, the low-end slopes of the mass function is the same for poor and rich haloes. In other words, if one used the Schechter (1976) parametrisation, $f(m) \propto m^{\alpha} \exp(-m/m_*)$, the exponential cutoff of the mass function, m_* , would be much lower for the poor systems, while the faint-end slope, α would be independent of richness.

3.3 The importance of mergers

Figure 8 shows the median value of the mass fraction f_{merg} accreted via mergers (instead of gas accretion) in different mass bins for the five models plotted in Figure 2a.

This median hides a large scatter, as one can see from the distribution of f_{merg} at constant m_{stars} in Figure 6, but shows a clear statistical trend. In the simple model with $m_{\text{stars}}^{\text{accr}} = f_b M_{\text{halo}}$ (dotted line), the median mass fraction accreted via mergers has a nearly constant value $f_{\text{merg}} \sim 0.5$ at $m_{\text{stars}} > 10^{10.5} h^{-1} M_{\odot}$. This is not surprising because in this model the baryons follow the dark matter, which is approximately scale free. The median mass fraction acquired by mergers is much lower for $m_{\text{stars}} < 10^{10.5} h^{-1} M_{\odot}$. This appears to be caused by the mass resolution of our dark matter simulation. Note that the host haloes of galaxies with $m_{\text{stars}} \sim 10^{10.5} h^{-1} M_{\odot}$ are well resolved. It is their merging histories that are not. Neglecting all mergers with sub-resolution haloes ($M_{\text{halo}} < 1.5 \times 10^9 h^{-1} M_{\odot}$) does not affect the value of f_{merg} for a cluster galaxy, but the effects of neglecting mergers with masses up to nearly the critical mass, $f_b M_{\text{shock}} = 1.3 \times 10^{11} h^{-1} M_{\odot}$.

Reionisation and supernova feedback (the terms in v_{circ} in Eq. 7) produce an effect analogous to that of the mass resolution by suppressing galaxy formation in all haloes below $v_{\text{circ}} = 40 \text{ km s}^{-1}$ and by considerably lowering the masses of galaxies in haloes just above this threshold. Therefore, mergers with small haloes make no or a very small contribution to the growth of the galaxy stellar mass, which results in a strong suppression of f_{merg} at all masses (Figure 8, short-dashed line).

The suppression of star formation at halo masses greater than M_{shock} has a small effect on the merging histories of galaxies with $M_{\text{halo}} \lesssim M_{\text{shock}}$, but it means that mergers provide the only mechanism for galaxies to grow above the limit mass $m_{\text{stars}} = m_{\text{crit}}$. Therefore, including the cut-off at M_{shock} increases the fractional importance of mergers in the growth of galaxies with $m_{\text{stars}} > m_{\text{crit}}$ (dash-dotted line relative to dotted line), not by affecting the merger rate but by decreasing the importance of gas accretion. Combining the terms in v_{circ} and M_{shock} causes: i) a strong suppression of the importance of mergers at $m_{\text{stars}} < m_{\text{crit}}$ and ii) a strong increase in the importance of mergers at $m_{\text{stars}} > m_{\text{crit}}$, both with respect to a simple model where the baryons follow the dark matter (dotted line). This explains the presence of two growth regimes, one dominated by gas accretion, the other dominated by mergers, respectively below and above $m_{\text{stars}} = m_{\text{crit}}$. Adding tidal stripping (solid line) has a minor effect on the median value f_{merg} , which may not be statistically significant.

Figure 6 shows that f_{merg} increases with m_{stars} along the relation for central galaxies. Figure 9 splits the mass accretion history of galaxies into three channels: 1) gas accretion, 2) *cold-mode* mergers (mergers that occur in haloes with $M_{\text{halo}}^{\text{host}} \leq M_{\text{shock}}$, and 3) *hot-mode* mergers (mergers that occur in haloes with $M_{\text{halo}}^{\text{host}} > M_{\text{shock}}$). Most galaxies with $m_{\text{stars}} > 10^{11} h^{-1} M_{\odot}$ have grown at least 40% of their mass via merging, and this merging involves almost always a primary halo more massive than M_{shock} . On the other hand, most galaxies with $m_{\text{stars}} < 10^{11} h^{-1} M_{\odot}$ have acquired most of their mass through gas accretion. Cold-mode mergers appear to contribute little to the growth of galaxies. In no mass bin is their median contribution to the final stellar mass more than $\sim 5\%$. This minor channel of galaxy mass growth reaches its maximum relative significance at a galaxy stellar mass of order $m_{\text{stars}} = f_b M_{\text{shock}}$.

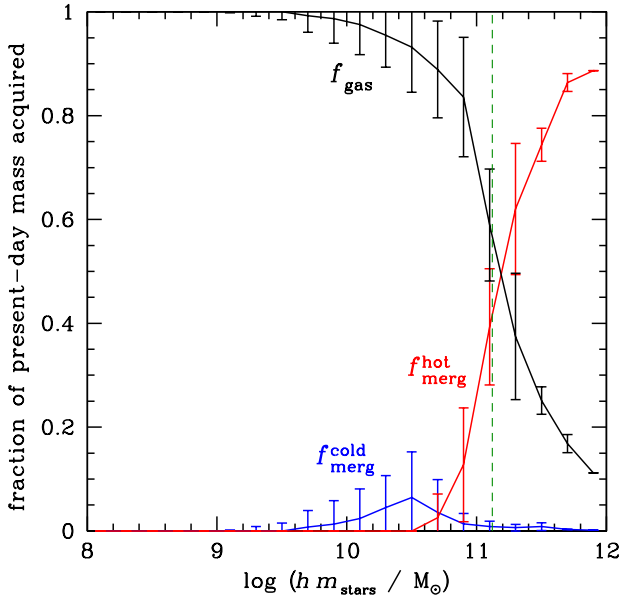


Figure 9. Median mass fraction at $z = 0$ acquired via gas accretion (black line), mergers within haloes with $M_{\text{halo}} < M_{\text{shock}}$ (cold-mode mergers, blue line), and mergers within haloes with $M_{\text{halo}} > M_{\text{shock}}$ (hot-mode mergers, red line). Error bars show the interquartile range. The green vertical dashed line shows the baryonic mass that corresponds to M_{shock} .

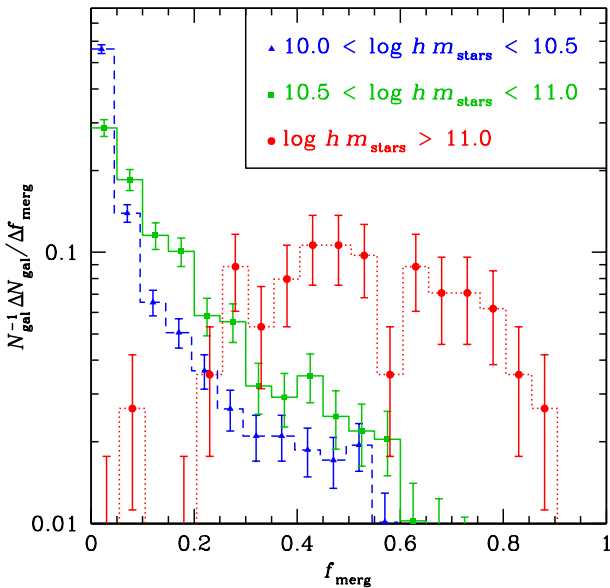


Figure 10. Distribution of fraction of the $z = 0$ mass acquired by mergers for galaxies in different bins of stellar mass.

Note that Figure 9 is virtually unchanged when we restrict ourselves to the central galaxies.

Still, some low mass galaxies do acquire most of their stellar mass via mergers. Figure 6 shows nearly one hundred central galaxies with host halo masses below M_{shock} that have acquired most of their stellar mass by mergers,

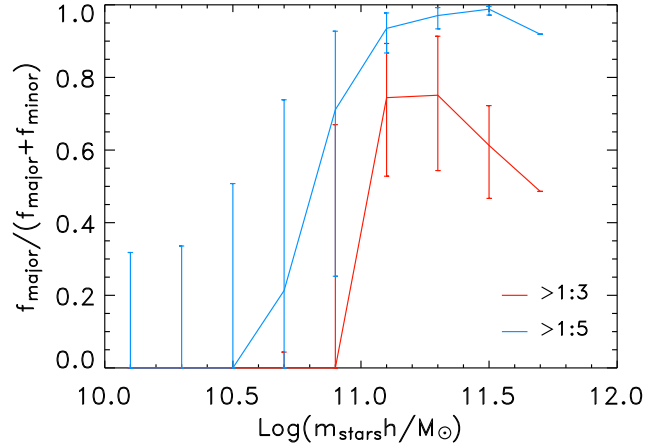


Figure 11. Fraction of the mass at $z = 0$ acquired by mergers due to major mergers. The red and blue curves show median values defining major mergers as mergers with stellar mass ratios larger than 1:3 and 1:5, respectively. The error bars show lower and upper quartiles. The points that corresponds to the bin of highest have no error bars because this bin contains one galaxy only.

more precisely by cold-mode mergers.⁴ Figure 10 shows the distribution of the fractional contribution of mergers to the final stellar mass for galaxies in four stellar mass intervals. A few galaxies that have accreted a significant fraction of their mass via mergers are present even in the lowest mass bin. In other words, by assuming that a large mass fraction acquired by mergers implies elliptical galaxy morphology (either through single major mergers or through repeated minor mergers, as suggested by Bournaud et al. 2007), our model can accommodate the presence of $10^{10.5} M_{\odot}$ galaxies with early type morphologies. However, the probability that a galaxy has an early type morphology (high f_{merg}) is much higher at $m_{\text{stars}} > 10^{11} h^{-1} M_{\odot}$ than it is at $10^{10} M_{\odot} < h m_{\text{stars}} < 10^{10.5} M_{\odot}$.

Figure 11 shows the contribution of major mergers to the total mass fraction at $z = 0$ acquired via mergers. We define major mergers as mergers with stellar mass ratios between 1:1 and 1:3. At $m_{\text{stars}} < 10^{11} h^{-1} M_{\odot}$ mergers have little importance and those that do occur are minor, while in galaxies with $m_{\text{stars}} \gtrsim 10^{11.2} h^{-1} M_{\odot}$ the greater contribution comes from major mergers (red line in Figure 11). Their dominance becomes overwhelming if we relax our definition of major mergers to include mergers with stellar mass ratios between 1:1 and 1:5.

It is not straightforward to interpret the increase in the relative importance of major mergers toward high masses. Naïvely, the steeper slope of the stellar mass function would indicate that major mergers are more important at low masses. Also, the finite mass resolution will prevent minor mergers at low masses, hence will give more importance to major mergers at the low-mass end. But Figure 11 shows

⁴ The large symbols for galaxies with high merger fractions in Figure 6 creates an illusion of the dominance of cold-mode mergers in low mass ($10 < \log h m_{\text{stars}} < 10.5$) central galaxies, which is dispelled in Figures 9 and 10.

instead that major mergers are enhanced at the high-mass end, except for the highest masses.

We suggest that the higher importance of major mergers at high galaxy masses is due to the slope of the $m_{\text{stars}} - M_{\text{halo}}$ relation in Figure 6, which flattens at high M_{halo} . Consider the merger of two haloes with $M_{\text{halo},2} \lesssim M_{\text{halo},1}$ and assume that this merger results in the merging of their galaxies, with masses $m_{\text{stars},2}$ and $m_{\text{stars},1}$. At low M_{halo} , where the relation is steep, $m_{\text{stars},2}/m_{\text{stars},1} \ll M_{\text{halo},2}/M_{\text{halo},1}$, but at high M_{halo} , where the relation flattens, $m_{\text{stars},2}/m_{\text{stars},1} > M_{\text{halo},2}/M_{\text{halo},1}$. Therefore, for a same spectrum of mass ratios for dark matter halo mergers, one expects that galaxy mergers become more minor at low masses and more major at high masses. This phenomenon predominates in driving the trend in Figure 11 until we reach the central galaxies of groups and clusters. Nearly equal mass mergers would require that they merged with other brightest cluster galaxies, but mergers of clusters are not so common events. This is why the relative contribution of major mergers tends to decrease again at $m_{\text{stars}} > 10^{11.2} h^{-1} M_{\odot}$.

4 DISCUSSION AND CONCLUSION

We have developed a *toy model* of galaxy formation, using a hybrid SAM/HOD approach to parametrise, as a function of halo mass and redshift, the stellar mass present in galaxies after gas accretion and quenching of gas infall by virial shocks and of star formation by reionisation and supernovae. We also include galaxy mergers, as derived from our high-resolution cosmological N-body simulation. The stellar mass acquired via gas accretion is modelled with a simple equation involving only three parameters, while we added a fourth parameter to describe the stellar mass loss caused by tidal stripping. We fine-tuned our four parameters to the observed stellar mass function of galaxies.

We have investigated the role of accretion, mergers and feedback in the growth of galaxies. In agreement with previous studies, we find that in all haloes, but more so in low ($M_{\text{halo}} \ll M_{\text{shock}}$) and high ($M_{\text{halo}} > M_{\text{shock}}$) mass haloes, $m_{\text{stars}}/M_{\text{halo}}$ must be much smaller than the universal cosmic baryon fraction if the halo mass function predicted by the CDM model is to be reconciled with the observed galaxy mass function.

The mechanism that suppresses star formation in haloes with $M_{\text{halo}} > M_{\text{shock}}$ is clear. The infalling gas is no longer able to radiate efficiently and is shock heated. The question is why this gas does not cool down again. Growing evidence suggests that this is due to heating from the central AGN (see Cattaneo et al. 2009; and references therein).

Reionisation and supernova feedback are widely invoked to explain the tiny stellar masses of galaxies in low mass haloes. The trouble is that attempts to simulate these processes have difficulty to produce outflows as large as those that are required by this study because the energy that is available is used inefficiently. However, unless the CDM model is wrong, whatever other process may be relevant must behave analogously to the reionisation and supernova feedback model described in the article, if it is to fit the same observational data that we have used.

The fact that $m_{\text{stars}}/M_{\text{halo}}$ drops below and above

M_{shock} introduces a characteristic scale for galaxy masses that makes them deviate from the dark matter's self-similar evolution (Marinoni & Hudson 2002; Baldry et al. 2008; Li & White 2009). If the evolution of baryons followed that of the dark matter, then galaxies of all masses would have similar merging histories. Instead, it is clear that the physics of the baryons, whatever they are, break the dark matter's scale-invariant behaviour by suppressing star formation in low and high-mass haloes. It is only within haloes in a narrow mass-range around $M_{\text{halo}} \sim M_{\text{shock}} \sim 10^{12} h^{-1} M_{\odot}$ that baryons can form stars efficiently (the galaxy formation zone).

Our very simple toy model of galaxy formation shows very distinct properties of central and satellite galaxies (see Fig. 6). The central galaxy masses increase slightly with halo mass, while the galaxy mass function, when measured within a narrow range of halo mass, will clearly separate the central and satellite populations, with a sharp bump for the high central masses (top panel of Fig. 7). This feature was first observed by Yang et al. (2009) in the SDSS survey, who also modelled it with the empirical conditional stellar mass function formalism. As we write these lines, we learnt that Liu et al. (2009) were also able to reproduce this behaviour with a semi-analytical model.

The suppression of galaxy formation in low-mass haloes reduces the importance of mergers as a mechanism for galaxy growth (dashed line in Figure 2 b), but the shut-down of gas accretion above the critical mass $M_{\text{shock}} \sim 10^{12} M_{\odot}$ implies that mergers are the only opportunity for galaxies to grow above the limiting mass $m_{\text{crit}} \equiv f_{\text{b}} M_{\text{shock}}$. Therefore, galaxies with $m_{\text{gal}} \gg m_{\text{crit}}$ must have acquired a significant fraction of their mass via mergers. In other words: mergers become important when gas accretion is quenched.

The present work reinforces the new picture in which galaxies grow through gas accretion and form stars along the *Blue Cloud* until the critical halo mass for shock heating is reached. Then gas accretion is shut off, star formation is quenched and they migrate to the *Red Sequence* (Cattaneo et al. 2006; Faber et al. 2007; Cattaneo et al. 2008). At this mass stage, mergers become important, so spiral galaxies are transformed into early type galaxies either by a major merger or by repeated minor mergers. Thus, we have a mechanism to explain why colour and morphological evolution go almost hand in hand.

We refer to mergers that take place in host haloes above M_{shock} as *hot-mode* mergers, and to mergers that take place in host haloes below M_{shock} as *cold-mode* mergers. The former usually contain little cold gas, while the latter involve galaxies containing large masses of cold gas supplied by cold accretion. It is thus tempting to identify hot-mode and cold-mode mergers with dry (dissipationless) and wet (gas-rich) mergers, respectively. The latter are mainly confined to galaxies below the critical stellar mass $f_{\text{b}} M_{\text{shock}}$ (Fig. 6) and are most frequent just below $f_{\text{b}} M_{\text{shock}}$ (Fig. 9). This points to a characteristic mass of $\sim 10^{10.5} h^{-1} M_{\odot}$ for ultraluminous infrared galaxies (ULIRGs, e.g. Colina et al. 2001) and quasar hosts (e.g. Bonoli et al. 2009), of which wet mergers are the supposed triggering mechanism (Figure 9).

Our model, therefore, predicts three regimes of galaxy formation. Galaxies with $m_{\text{stars}} \lesssim 10^{10} M_{\odot}$ were effectively built up by gas accretion only. At $10^{10} M_{\odot} \lesssim m_{\text{stars}} \lesssim 10^{11} M_{\odot}$ gas accretion remains the

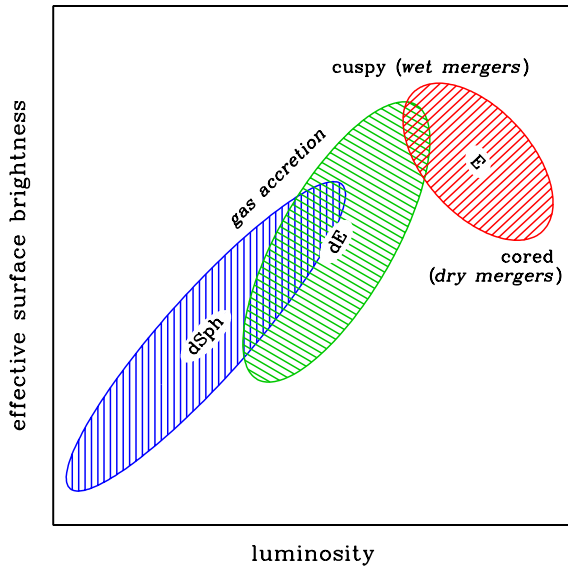


Figure 12. A qualitative description of the distribution of different types of red galaxies on the luminosity - surface brightness plane (see Kormendy et al. 2009 and Mateo 1998 for actual data). “True” ellipticals (merger remnants) form a sequence (shown in red) where the surface brightness decreases with luminosity. This is because low-mass ellipticals were formed in wet mergers, which drove plenty of gas to the centre. This gas formed central stellar cusps that are responsible for the high surface brightness of these galaxies. High-mass ellipticals were formed in dry mergers, where the cusps were whittled out by the scattering action of two supermassive black holes (especially in the common major mergers), leading to a decrease in surface brightness. In contrast, the great majority of the galaxies that are commonly known as dEs (Sphs in the classification by Kormendy et al. 2009) form a sequence (shown in green) where surface brightness increases with galaxy masses. At lower luminosities, the dE sequence extends that formed by the dSphs in the Local Group (shown in blue). This is because dSphs and dEs are galaxies that were built by gas accretion rather than mergers. Galaxies that are more massive have higher surface brightness because they started to form earlier, when the Universe was denser, and because they were less affected by stellar feedback. The reversal of the trend of surface brightness with luminosity around the critical mass is another sign of the transition from a galaxy formation regime dominated by gas accretion and stellar feedback to another regime dominated by dry mergers and the action of supermassive black holes.

dominant mechanism, but we also see a population that was built by wet mergers. Galaxies with $m_{\text{stars}} \gtrsim 10^{11} \odot$ were built by dry mergers. Galaxies built by wet mergers are rare at all masses.

Based on computer simulations (Ebisuzaki et al. 1991; Barnes & Hernquist 1991; Cox et al. 2006; Naab et al. 2007) and observations of the structural properties of elliptical galaxies (Faber et al. 1997; Kormendy et al. 2009), the galaxies built by dry mergers at $m_{\text{stars}} \gtrsim 10^{11} \odot$ correspond to the population of ellipticals with quasi-homogeneous cores. The galaxies built by wet mergers at $10^{10} M_{\odot} \lesssim m_{\text{stars}} \lesssim 10^{11} \odot$ correspond to the population of cuspy ellipticals. The galaxies built by gas accretion at $m_{\text{stars}} \lesssim 10^{11} \odot$ comprise spiral galaxies, but they must also

comprise other morphological types for the reason that we are about to explain.

Over three quarters of the galaxies in clusters, the huge majority of which are satellites, lie on the Red Sequence (Yang et al. 2008)⁵, which is visible to very low luminosities (e.g. Boué et al. 2008) and is mainly composed of galaxies with early-type morphologies, the great majority of which are classified as dwarf ellipticals (dEs). On a mass - surface brightness diagram, most of the galaxies classified as dE populate a sequence that is orthogonal to that formed by cuspy and core ellipticals, although it is aligned with the mass - surface brightness relation of dwarf spheroidal (dSph) galaxies in the Local Group. Only a few dEs lie on the mass - surface brightness relation of cuspy and core ellipticals. Kormendy et al. (2009) interpret this dichotomy as a distinction between “true” ellipticals formed by galaxy mergers (wet for cuspy ellipticals, dry for core ellipticals) and galaxies whose at first sight similar morphological properties have in fact a different origin. They, therefore, propose to rename spheroidals (Sphs) the dEs that do not lie on the mass - surface brightness relation of Es, but rather continue to higher masses the mass - surface brightness relation of dSphs. Fig. 6 strongly supports this interpretation by showing that, except the few most massive galaxies, the population of cluster galaxies was not built by mergers. We, therefore, must conclude that the morphological properties and the shutdown of star formation in dEs and dSphs are due to processes unrelated to mergers, i.e. ram-pressure stripping, strangulation and harassment by repeated fast encounters (Moore et al. 1998; Mastropietro et al. 2005).

Figs. 6 and 9 show that mergers are the major contributor to the growth of the most massive galaxies, e.g. the central galaxies of groups and clusters. Maller et al. (2006) reached a similar conclusion from hydrodynamic cosmological simulations. However, their simulations lack effective feedback and substantially overestimate the observed galaxy mass function. Therefore, they overestimated the role of gas accretion. Nevertheless, they did determine that the average number of both minor and major mergers increases with m_{stars} . They found that a high-mass galaxy has typically undergone one major merger through its lifetime. We go one step further. Not only do we find that mergers are common among the most massive galaxies. We also find that the masses of these galaxies were mainly built by mergers.

Naab et al. (2007) also used hydrodynamic simulations to address the importance of mergers. However, in contrast with Maller et al. (2006), who simulated a cosmic volume at low resolution, they used very high resolution to zoom into the formation of three individual ellipticals. They found their galaxies have grown by mergers from $z = 1$ to $z = 0$ by 25% in mass on average. They, therefore, concluded that the masses of M_* elliptical galaxies were not built by major mergers. We note, however, that their three ellipticals accreted over half of their mass by mergers since $z = 5$.

⁵ The 22% of non-Red Sequence cluster galaxies found by Yang et al. (2008) matches perfectly the fraction of interlopers projected along the virial sphere, i.e. the average fraction of particles in the virial cone that are outside the virial sphere (Mamon et al. 2010). Hence, the fraction of non-Red Sequence galaxies within the virial sphere is probably much lower than one-quarter.

Moreover, at $z = 0$, these galaxies live in haloes with virial masses in the range of $1.6 - 2.3 \times 10^{12} M_{\odot}$. This is precisely the mass range where the importance of mergers begins to be comparable to that of gas accretion, while the importance of major mergers is small (Fig. 11). We therefore find the agreement between our results and those by Naab et al. (2007) quite encouraging.

Much higher mass resolution on our side would certainly be desirable to follow properly substructures until they have merged with their hosts. However, this problem has been partly handled with the incorporation of delayed merging on a dynamical friction timescale (Sect. 2.2). Moreover, our low v_{circ} cut-off implies that there is not much advantage at resolving haloes with masses that are much lower than the mass at which $v_{\text{circ}} = v_{\text{reion}}$ because there is no formation of galaxies in those haloes.

What we believe to be significant is that even after correcting for overmerging, we still have an excess of massive galaxies compared to the Bell et al. (2003) mass function (dotted line in Figure 2a). This remains true for other determinations of the galaxy stellar mass function. One could argue that, although the semianalytic model that we use for the merger time is a good match to what is seen in hydrodynamic simulations (Jiang et al. 2008), we may still overestimate the galaxy merger rate, which is still somewhat uncertain. However, it is difficult to lower the merger rate without overproducing low-mass galaxies (see the dashed line in Figure 2a). One could imagine compensating for this effect by increasing feedback at low masses, but we could not find a plausible parameter set that does this and fits the galaxy mass function as well as the full model in Figure 2 does.

While we do not claim to have explored all possible parameter combinations, any model that suppresses star formation even further will worsen our agreement with the normalisation of the cosmic SFR density (Figure 5). We also note that the tendency to be at the lower limit of the observational range for the cosmic SFR density is not specific to our model, since it is also found in state-of-the-art semianalytic models that are based on the same fundamental assumptions (see Figure 8 in Cattaneo et al. 2006).

We believe that tidal stripping and observational errors in the SDSS magnitudes that anchor the top end of the Bell et al. (2003) mass function (which according to Lauer et al. 2007 can run up to a magnitude) can easily reconcile our model with the top end of the galaxy stellar mass function. The fundamental reason why the magnitudes of bright ellipticals are difficult to measure is that their shallow light profiles do not converge. So it is hard to estimate the total light, let alone distinguish galaxy light from intracluster light (see the discussion in the Appendix A of Cattaneo et al. 2008). Since the extended envelopes of massive ellipticals are probably the products of interactions, the distinction between the full model and the full model without stripping may be one more of name than of substance. If we decide that the envelopes belong to the galaxies, then we should conclude that the full model without stripping is correct and that the problem lies with the data, which are likely to underestimate the real masses. If instead we decide that the envelopes are intracluster light, then we should conclude that the model that includes tidal stripping is the most physical one. For our best fit value $\eta_{\text{strip}} = 0.4$, the stripped mass in haloes with $M_{\text{halo}} \sim 10^{13} - 10^{14} h^{-1} M_{\odot}$ is in the

range of $\sim 0.05 - 0.1 f_b M_{\text{halo}}$. This value is consistent with a number of independent measurements that place a 10–20% lower limit to the fraction of diffuse light in clusters with respect to the amount of light in individual galaxies (see Arnaboldi 2004 for a review).

An important caveat to this article is that our model does not describe star formation, as we are only interested in the total mass of a galaxy and the fraction of this mass that comes from mergers. This paper is not concerned with the fraction of the mass that is in gas and the fraction of the mass that is in stars. The SFRs that we show (Figure 5) are simply mass accretion rates that are estimated assuming that all the accreted gas is instantaneously turned into stars. In practice, at redshift $z \sim 0$, where we compare our model with the data (Figures 2a and 6), the gas is usually a small fraction of the galaxy mass. Therefore, the error that we make by identifying the stellar mass with the total galaxy mass (stars plus cold gas) is at most $\sim 10 - 20\%$, which is compatible with the level of accuracy that we expect from our model. We note that even observationally, the cosmic SFR density derived from dust-corrected measured SFRs deviates at $z > 1$ from the time derivative of the cosmic stellar mass density (Wilkins et al. 2008; Figure 5). The origin of this discrepancy is an open problem. Our model agrees with the observed time derivative of the cosmic stellar mass density better than it does with the measured star formation rate density.

Still many questions remain. Our model predicts that most elliptical galaxies did not first merge and then stop making stars. They rather first entered the hot-mode regime and then grew by dry mergers. Ceasing to accrete gas is not the same as having exhausted one's entire gas reservoir, although simulations suggest that when gas accretion stops, the end of star formation is near (e.g. Cattaneo et al. 2007). This could be trouble because it is only in cold-mode mergers that there is gas for fuelling the growth of supermassive black holes. If the formation of ellipticals has mainly occurred via hot mode (dry) mergers in haloes with $M_{\text{halo}} > M_{\text{shock}}$, why is there a well-defined relation between black holes and spheroids (Magorrian et al. 1998)?

Mergers are a reality and we have tried to present a careful and robust estimate of their importance. Our work suggests that present-day giant ellipticals can only be built by dry mergers, as gas accretion is quenched at high halo mass. This conclusion is consistent with the structural properties of giant ellipticals, which point to a dissipationless origin (Naab et al. 2006; Kormendy et al. 2009), and to the higher numbers of galaxy mergers per Gyr found for massive galaxies by Maller et al. (2006). The question is whether mergers are the only process responsible for the formation of elliptical galaxies, particularly when it comes to proto-ellipticals at high redshift (e.g. Dekel et al. 2009).

ACKNOWLEDGEMENTS

AC and GAM acknowledge interesting conversations with A. Dekel, S.M. Faber, J. Silk, and D. Tweed. We also thank A. Hopkins for providing the observational data for Figure 5. AK is supported by the MICINN through the Ramon y Cajal programme. KW acknowledges support through the DFG grant KN 755/1.

REFERENCES

- Arnaboldi, M. 2004, in *Baryons in Dark Matter Halos*, ed. R. Dettmar, U. Klein, & P. Salucci
- Arnouts, S., Schiminovich, D., Ilbert, O., et al. 2005, *ApJL*, 619, L43
- Baldry, I. K., Glazebrook, K., Budavári, T., et al. 2005, *MNRAS*, 358, 441
- Baldry, I. K., Glazebrook, K., & Driver, S. P. 2008, *MNRAS*, 388, 945
- Barger, A. J., Cowie, L. L., & Richards, E. A. 2000, *AJ*, 119, 2092
- Barnes, J. E. & Hernquist, L. E. 1991, *ApJL*, 370, L65
- Bell, E. F. & de Jong, R. S. 2001, *ApJ*, 550, 212
- Bell, E. F., McIntosh, D. H., Katz, N., & Weinberg, M. D. 2003, *ApJS*, 149, 289
- Berlind, A. A. & Weinberg, D. H. 2002, *ApJ*, 575, 587
- Binney, J. & Tremaine, S. 2008, *Galactic Dynamics: Second Edition* (Princeton University Press, Princeton, NJ USA)
- Birnbom, Y. & Dekel, A. 2003, *MNRAS*, 345, 349
- Blanchard, A., Valls-Gabaud, D., & Mamon, G. A. 1992, *A&A*, 264, 365
- Blumenthal, G. R., Faber, S. M., Primack, J. R., & Rees, M. J. 1984, *Nature*, 311, 517
- Bonoli, S., Marulli, F., Springel, V., et al. 2009, *MNRAS*, 396, 423
- Boué, G., Adami, C., Durret, F., Mamon, G. A., & Cayatte, V. 2008, *A&A*, 479, 335
- Bournaud, F., Jog, C. J., & Combes, F. 2007, *A&A*, 476, 1179
- Bouwens, R. 2006, in *The Fabulous Destiny of Galaxies: Bridging Past and Present*, ed. V. Le Brun, A. Mazure, S. Arnouts, & D. Burgarella, 373
- Bouwens, R., Broadhurst, T., & Illingworth, G. 2003, *ApJ*, 593, 640
- Bower, R. G., Benson, A. J., Malbon, R., et al. 2006, preprint astro-ph/0511338
- Bryan, G. L. & Norman, M. L. 1998, *ApJ*, 495, 80
- Bunker, A. J., Stanway, E. R., Ellis, R. S., & McMahon, R. G. 2004, *MNRAS*, 355, 374
- Cattaneo, A. 2001, *MNRAS*, 324, 128
- Cattaneo, A., Blaizot, J., Weinberg, D. H., et al. 2007, *MNRAS*, 377, 63
- Cattaneo, A., Dekel, A., Devriendt, J., Guiderdoni, B., & Blaizot, J. 2006, *MNRAS*, 370, 1651
- Cattaneo, A., Dekel, A., Faber, S. M., & Guiderdoni, B. 2008, *MNRAS*, 389, 567
- Cattaneo, A., Faber, S. M., Binney, J., et al. 2009, *Nature*, 460, 213
- Chandrasekhar, S. 1943, *ApJ*, 97, 255
- Cole, S., Aragon-Salamanca, A., Frenk, C. S., Navarro, J. F., & Zepf, S. E. 1994, *MNRAS*, 271, 781
- Colina, L., Borne, K., Bushouse, H., et al. 2001, *ApJ*, 563, 546
- Condon, J. J. 1989, *ApJ*, 338, 13
- Condon, J. J., Cotton, W. D., & Broderick, J. J. 2002, *AJ*, 124, 675
- Connolly, A. J., Szalay, A. S., Dickinson, M., Subbarao, M. U., & Brunner, R. J. 1997, *ApJL*, 486, L11+
- Cowie, L. L., Songaila, A., & Barger, A. J. 1999, *AJ*, 118, 603
- Cox, T. J., Dutta, S. N., Di Matteo, T., et al. 2006, *ApJ*, 650, 791
- Croton, D. J., Springel, V., White, S. D. M., et al. 2006, *MNRAS*, 365, 11
- Dekel, A. & Birnboim, Y. 2006, *MNRAS*, 368, 2
- Dekel, A., Birnboim, Y., Engel, G., et al. 2009, *Nature*, 457, 451
- Dekel, A. & Silk, J. 1986, *ApJ*, 303, 39
- Ebisuzaki, T., Makino, J., & Okumura, S. K. 1991, *Nature*, 354, 212
- Efstathiou, G. 1992, *MNRAS*, 256, 43P
- Efstathiou, G., Davis, M., White, S. D. M., & Frenk, C. S. 1985, *ApJS*, 57, 241
- Faber, S. M., Tremaine, S., Ajhar, E. A., et al. 1997, *AJ*, 114, 1771
- Faber, S. M., Willmer, C. N. A., Wolf, C., et al. 2007, *ApJ*, 665, 265
- Fall, S. M. & Efstathiou, G. 1980, *MNRAS*, 193, 189
- Flores, H., Hammer, F., Thuan, T. X., et al. 1999, *ApJ*, 517, 148
- Gallego, J., García-Dabó, C. E., Zamorano, J., Aragón-Salamanca, A., & Rego, M. 2002, *ApJL*, 570, L1
- Gallego, J., Zamorano, J., Aragon-Salamanca, A., & Rego, M. 1995, *ApJL*, 455, L1
- Georgakakis, A., Hopkins, A. M., Sullivan, M., et al. 2003, *MNRAS*, 345, 939
- Ghigna, S., Moore, B., Governato, F., et al. 1998, *MNRAS*, 300, 146
- Giavalisco, M., Dickinson, M., Ferguson, H. C., et al. 2004, *ApJL*, 600, L103
- Gill, S. P. D., Knebe, A., & Gibson, B. K. 2004, *MNRAS*, 351, 399
- Glazebrook, K., Blake, C., Economou, F., Lilly, S., & Colless, M. 1999, *MNRAS*, 306, 843
- Gnedin, N. Y. 2000, *ApJ*, 542, 535
- Gross, M. A. K. 1997, PhD thesis, University of California, Santa Cruz)
- Haarsma, D. B., Partridge, R. B., Windhorst, R. A., & Richards, E. A. 2000, *ApJ*, 544, 641
- Hammer, F., Flores, H., Lilly, S. J., et al. 1997, *ApJ*, 481, 49
- Hanish, D. J., Meurer, G. R., Ferguson, H. C., et al. 2006, *ApJ*, 649, 150
- Hayashi, E., Navarro, J. F., Taylor, J. E., Stadel, J., & Quinn, T. 2003, *ApJ*, 584, 541
- Hogg, D. W., Cohen, J. G., Blandford, R., & Pahre, M. A. 1998, *ApJ*, 504, 622
- Hopkins, A. M. 2004, *ApJ*, 615, 209
- Hopkins, A. M. & Beacom, J. F. 2006, *ApJ*, 651, 142
- Hopkins, A. M., Connolly, A. J., & Szalay, A. S. 2000, *AJ*, 120, 2843
- Jiang, C. Y., Jing, Y. P., Faltenbacher, A., Lin, W. P., & Li, C. 2008, *ApJ*, 675, 1095
- Kauffmann, G., White, S. D. M., & Guiderdoni, B. 1993, *MNRAS*, 264, 201
- Kazantzidis, S., Mayer, L., Mastropietro, C., et al. 2004, *ApJ*, 608, 663
- Kitayama, T. & Suto, Y. 1996, *ApJ*, 469, 480
- Klimentowski, J., Lokas, E. L., Kazantzidis, S., Mayer, L., & Mamon, G. A. 2009, *MNRAS*, 397, 2015
- Knollmann, S. R. & Knebe, A. 2009, *ApJS*, 182, 608
- Komatsu, E., Dunkley, J., Nolte, M. R., et al. 2009, *ApJS*, 180, 330

- Kormendy, J., Fisher, D. B., Cornell, M. E., & Bender, R. 2009, *ApJS*, 182, 216
- Kravtsov, A. V., Gnedin, O. Y., & Klypin, A. A. 2004, *ApJ*, 609, 482
- Kroupa, P. 2002, *Science*, 295, 82
- Lacey, C. & Cole, S. 1993, *MNRAS*, 262, 627
- Lauer, T. R., Gebhardt, K., Faber, S. M., et al. 2007, *ApJ*, 664, 226
- Le Floch, E., Papovich, C., Dole, H., et al. 2005, *ApJ*, 632, 169
- Li, C. & White, S. D. M. 2009, *MNRAS*, 398, 2177
- Liu, L., Yang, X., Mo, H. J., van den Bosch, F. C., & Springel, V. 2009, *ApJ*, submitted, arXiv:0912.1257
- Lo Faro, B., Monaco, P., Vanzella, E., et al. 2009, *MNRAS*, 399, 827
- Macciò, A. V., Dutton, A. A., & van den Bosch, F. C. 2008, *MNRAS*, 391, 1940
- Machalski, J. & Godlowski, W. 2000, *A&A*, 360, 463
- Magorrian, J., Tremaine, S., Richstone, D., et al. 1998, *AJ*, 115, 2285
- Maller, A. H., Katz, N., Kereš, D., Davé, R., & Weinberg, D. H. 2006, *ApJ*, 647, 763
- Mamon, G. A. 1992, *ApJL*, 401, L3
- Mamon, G. A., Biviano, A., & Murante, G. 2010, *A&A*, submitted
- Marinoni, C. & Hudson, M. J. 2002, *ApJ*, 569, 101
- Massarotti, M., Iovino, A., & Buzzoni, A. 2001, *ApJL*, 559, L105
- Mastropietro, C., Moore, B., Mayer, L., et al. 2005, *MNRAS*, 364, 607
- Mateo, M. L. 1998, *ARA&A*, 36, 435
- Mauch, T. & Sadler, E. M. 2007, *MNRAS*, 375, 931
- McQuinn, M., Lidz, A., Zaldarriaga, M., et al. 2009, *ApJ*, 694, 842
- Moore, B., Lake, G., & Katz, N. 1998, *ApJ*, 495, 139
- Moorwood, A. F. M., van der Werf, P. P., Cuby, J. G., & Oliva, E. 2000, *A&A*, 362, 9
- Naab, T., Jesseit, R., & Burkert, A. 2006, *MNRAS*, 372, 839
- Naab, T., Johansson, P. H., Ostriker, J. P., & Efstathiou, G. 2007, *ApJ*, 658, 710
- Nakamura, T. T. 1996, Master's thesis, Univ. of Tokyo
- Navarro, J. F., Frenk, C. S., & White, S. D. M. 1996, *ApJ*, 462, 563
- Neistein, E. & Dekel, A. 2008, *MNRAS*, 383, 615
- Neistein, E. & Weinmann, S. M. 2009, *MNRAS*, submitted, arXiv:0911.3147
- Ouchi, M., Shimasaku, K., Okamura, S., et al. 2004, *ApJ*, 611, 660
- Pérez-González, P. G., Gallego, J., Zamorano, J., et al. 2003, *ApJL*, 587, L27
- Pérez-González, P. G., Rieke, G. H., Egami, E., et al. 2005, *ApJ*, 630, 82
- Pettini, M., Kellogg, M., Steidel, C. C., et al. 1998, *ApJ*, 508, 539
- Sadler, E. M., Jackson, C. A., Cannon, R. D., et al. 2002, *MNRAS*, 329, 227
- Salpeter, E. E. 1955, *ApJ*, 121, 161
- Schechter, P. 1976, *ApJ*, 203, 297
- Schiminovich, D., Ilbert, O., Arnouts, S., et al. 2005, *ApJL*, 619, L47
- Serjeant, S., Gruppioni, C., & Oliver, S. 2002, *MNRAS*, 330, 621
- Silk, J. & Rees, M. J. 1998, *A&A*, 331, L1
- Somerville, R. S., Hopkins, P. F., Cox, T. J., Robertson, B. E., & Hernquist, L. 2008, *MNRAS*, 391, 481
- Somerville, R. S. & Kolatt, T. S. 1999, *MNRAS*, 305, 1
- Springel, V. 2005, *MNRAS*, 364, 1105
- Steidel, C. C., Adelberger, K. L., Giavalisco, M., Dickinson, M., & Pettini, M. 1999, *ApJ*, 519, 1
- Sullivan, M., Treyer, M. A., Ellis, R. S., et al. 2000, *MNRAS*, 312, 442
- Teplitz, H. I., Collins, N. R., Gardner, J. P., Hill, R. S., & Rhodes, J. 2003, *ApJ*, 589, 704
- Thompson, R. I., Eisenstein, D., Fan, X., et al. 2006, *ApJ*, 647, 787
- Thoul, A. A. & Weinberg, D. H. 1996, *ApJ*, 465, 608
- Toomre, A. 1977, in *The Evolution of Galaxies and Stellar Populations*, ed. B. M. Tinsley & R. B. Larson (New Haven: Yale University Press), 401–416
- Tresse, L. & Maddox, S. J. 1998, *ApJ*, 495, 691
- Tresse, L., Maddox, S. J., Le Fèvre, O., & Cuby, J.-G. 2002, *MNRAS*, 337, 369
- Treyer, M. A., Ellis, R. S., Milliard, B., Donas, J., & Bridges, T. J. 1998, *MNRAS*, 300, 303
- White, S. D. M. & Frenk, C. S. 1991, *ApJ*, 379, 52
- White, S. D. M. & Rees, M. J. 1978, *MNRAS*, 183, 341
- Wilkins, S. M., Trentham, N., & Hopkins, A. M. 2008, *MNRAS*, 385, 687
- Wilson, G., Cowie, L. L., Barger, A. J., & Burke, D. J. 2002, *AJ*, 124, 1258
- Wolf, C., Wisotzki, L., Borch, A., et al. 2003, *A&A*, 408, 499
- Yan, L., McCarthy, P. J., Freudling, W., et al. 1999, *ApJL*, 519, L47
- Yang, X., Mo, H. J., & van den Bosch, F. C. 2003, *MNRAS*, 339, 1057
- Yang, X., Mo, H. J., & van den Bosch, F. C. 2008, *ApJ*, 676, 248
- Yang, X., Mo, H. J., & van den Bosch, F. C. 2009, *ApJ*, 695, 900